

The ELT/METIS Annular Groove Phase Masks

Christian Delacroix^{*a}, Lorenzo König^{a,b}, Olivier Absil^a, Gilles Orban De Xivry^a, Pontus Forsberg^c, Mikael Karlsson^c, Samuel Ronayette^d, Eric Pantin^d, and Jean-Christophe Barrière^d

^aSTAR Institute, University of Liège, Belgium

^bJet Propulsion Laboratory, California Institute of Technology, 4800 Oak Grove Dr, Pasadena 91109 CA, US

^cDepartment of Materials Science and Engineering, Uppsala University, Sweden

^dUniversité Paris-Saclay, CEA, Gif-sur-Yvette, France

ABSTRACT

High-contrast imaging instruments use coronagraphs for studying stellar environments by suppressing the intense glare of stars. The Annular Groove Phase Mask (AGPM), a vector vortex coronagraph, has proven to be a valuable tool, offering high-contrast performance at small angular separations. The Mid-infrared ELT Imager and Spectrograph (METIS) project will incorporate multiple AGPMs designed to operate at various wavelengths within the LMN spectral bands. Recently, the METIS project has entered the Manufacture, Assembly, Integration, and Test (MAIT) phase. During MAIT, the AGPMs, referred to as Vortex Phase Masks (VPMs) in the framework of METIS, are subject to an iterative process of manufacturing and testing. In the event of performance discrepancies, a component undergoes a minor re-etching process and is subsequently re-tested until it meets the specified requirements. In this work, we evaluate the performance of the METIS VPMs on two distinct coronagraphic test benches. On one hand, the Vortex Optical Demonstrator for Coronagraphic Applications (VODCA) at the University of Liège, featuring a supercontinuum laser source and a FLIR infrared camera, is employed to assess the METIS L- and M-band VPMs. On the other hand, the performance of the METIS N-band VPMs is assessed using a cryogenic testbed at CEA Paris-Saclay. This second testbed is equipped with a series of lasers spanning the 8 to $12.5\mu\text{m}$ range, ensuring high wavefront quality with a single-mode output. We present the outcome of our extensive manufacturing and testing campaigns and reveal the measured coronagraphic performance results for all METIS VPMs.

Keywords: high-contrast imaging, annular groove phase mask, vortex coronagraph, laboratory demonstration, ELT/METIS, mid-infrared instrumentation

1. INTRODUCTION

High-contrast imaging (HCI) instruments, such as the Mid-infrared ELT Imager and Spectrograph (METIS), utilize coronagraphs to study stellar environments by suppressing the intense glare of stars. One key component of these instruments is the Annular Groove Phase Mask (AGPM¹), a type of vector vortex coronagraph known for its high-contrast performance at small angular separations. In the framework of METIS, these AGPMs are referred to as Vortex Phase Masks (VPMs), and they are designed to operate across the LMN spectral bands, covering wavelengths from 2.9 to $13.1\mu\text{m}$.

METIS HCI objectives impose specific performance requirements on the vortex coronagraph, thereby setting stringent criteria for the VPMs. The primary requirement for the VPMs is that they should not limit the achievable contrast after postprocessing, which is validated by comprehensive end-to-end simulations.^{2,3} Detailed in the METIS Final Design Review^{4,5} documentation, the requirements for the L and M bands include an average null depth below 2×10^{-3} and a peak null depth below 1×10^{-2} at each individual wavelength. For the N band, which is also limited by the significant impact of water vapor seeing⁶ on the error budget, the criteria are less demanding, with an average null depth below 1×10^{-2} and a peak null depth below 5×10^{-2} at each wavelength.

*cdelacroix@uliege.be

Recently, the METIS project has entered the Manufacture, Assembly, Integration, and Test (MAIT) phase. During MAIT, the VPMs undergo an iterative process of manufacturing and testing. The VPMs for METIS are made from polycrystalline diamond. VPM-L and VPM-M have a diameter of 20mm , providing a sufficiently large field of view. VPM-N are smaller, 15mm in diameter, to accommodate the placement of three VPMs side by side in the focal plane to facilitate chopping. If performance discrepancies are found, the components undergo a minor re-etching process and are re-tested until they meet the specified requirements.

This work evaluates the performance of the VPMs manufactured for METIS. In Sec. 2, we present the design optimization and the manufacturing of the VPMs. Sec. 3 is dedicated to the testing of VPM-L and VPM-M at the University of Liège, on a dedicated coronagraphic bench. Finally, in Sec. 4, we present the performance of the N-band VPMs, evaluated using a cryogenic testbed at CEA Paris-Saclay.

2. DESIGN AND MANUFACTURING

The METIS VPMs are made using the AGPM technology, which means they feature concentric annular grooves etched into a diamond substrate, creating a phase shift that enables the cancellation of starlight through destructive interference while allowing light from off-axis sources, like exoplanets, to pass through. The phase shift $\Delta\Phi_{\text{TE-TM}}$ is obtained thanks to the property of form birefringence of the grating, which gives two different refractive indices n_{TE} (transverse electric) and n_{TM} (transverse magnetic):

$$\Delta\Phi_{\text{TE-TM}}(\lambda) = \frac{2\pi}{\lambda} h \Delta n_{\text{form}}(\lambda) \quad (1)$$

where h is the grating depth, and

$$\Delta n_{\text{form}}(\lambda) = (n_{\text{TE}} - n_{\text{TM}}). \quad (2)$$

The form birefringence is engineered to (partially) compensate for the $1/\lambda$ dependence of the phase shift across a significant range of wavelengths.⁷ This technology is particularly adapted to making VPMs achromatic over broad spectral bandwidths at infrared wavelengths.

The design of the VPM grating parameters was closely coordinated with the manufacturing process, using realistic numerical simulations based on rigorous coupled wave analysis (RCWA), a reliable simulation tool for achieving the required contrast levels for METIS. While a perfect achromatic coronagraph theoretically nullifies on-axis starlight, practical imperfections remain. The theoretical null depth, measuring contrast across the point spread function (PSF), is given by:

$$N_{\text{theo}}(\lambda) = \frac{I_{\text{coro}}(\lambda)}{I_{\text{off}}(\lambda)} = \frac{\left[1 - \sqrt{q(\lambda)}\right]^2 + \epsilon(\lambda)^2 \sqrt{q(\lambda)}}{\left[1 + \sqrt{q(\lambda)}\right]^2} \quad (3)$$

where I_{coro} (resp. I_{off}) is the signal intensity when the input beam is centred on (resp. off) the coronagraph, $\epsilon(\lambda)$ is the phase error with respect to π , and $q(\lambda)$ is the flux ratio between the two polarisation components, TE and TM.

The expected null depth for all METIS VPMs is illustrated in Fig. 1. The ideal case where the ghost signal is not included is compared to the realistic case with a minimal ghost, almost totally cancelled by the antireflective grating as described in Sec. 3.2. For the operating wavelengths of VPM-L ($2.9 - 4.1\mu\text{m}$) and VPM-M ($3.9 - 5.3\mu\text{m}$) bands, grating parameters are designed to achieve null depths below 10^{-3} , except at the band edges where slight performance reductions are deemed acceptable. Tolerances on these parameters were shown to be tight but manageable, with adjustments in one parameter (grating depth) compensating for deviations in others (particularly sidewall angles). In the case of the M band, its narrower relative bandwidth compared to L band leads to slightly improved performance and relaxed manufacturing tolerances.

Early in the project, we targeted the same level of performance at N band as at LM bands, necessitating subdivision into N1 ($8.0 - 10.5\mu\text{m}$) and N2 ($10.0 - 13.5\mu\text{m}$) subbands, each optimized separately. After assessing the end-to-end performance of N-band vortex coronagraphy,^{3,5} it was found that the VPM performance could

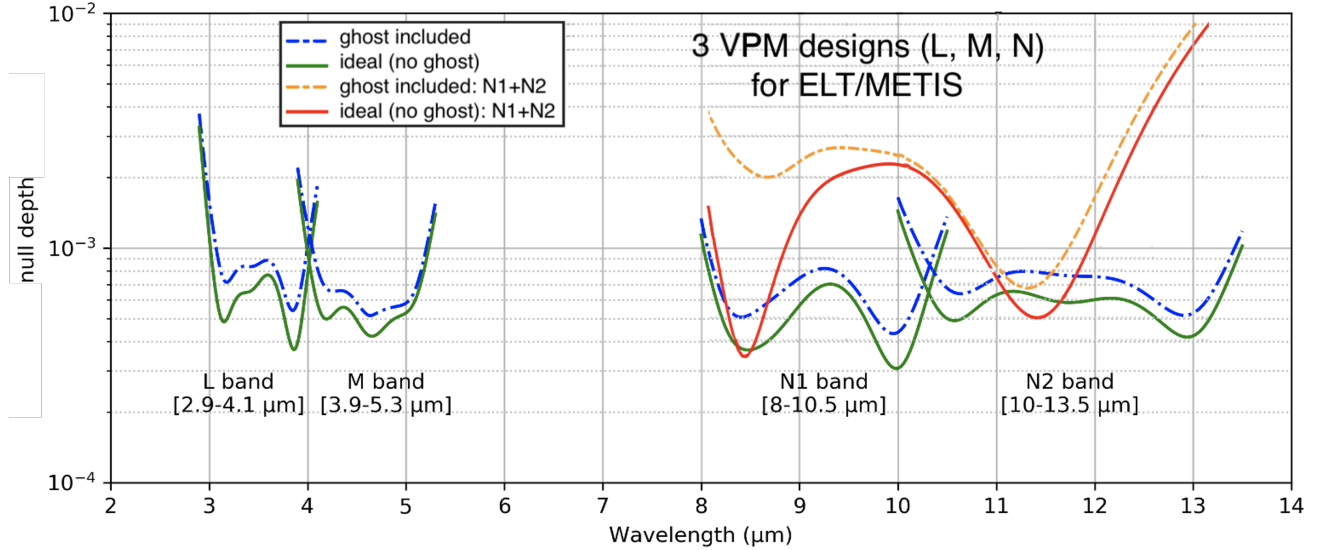


Figure 1. Null depth of all METIS VPMs optimized with RCWA: theoretical null depth without internal reflections (solid line) and realistic null depth including the faint ghost signal (almost canceled by the antireflective grating, dashed line). The graph also shows the null depth curves obtained for the initially proposed N1 and N2 subbands, replaced by a single VPM-N design (orange and red lines).

be relaxed to the values already quoted above, which allowed to move to a single-VPM implementation as a cost-effective alternative to initial dual VPMs. This consolidation reduces the number of required VPMs from 6 to 3 for the N band, considering that vortex operations at N band need to be compatible with a three-point chopping pattern. Tab. 1 summarizes the design optimization parameters for all METIS VPMs, used to produce Fig. 1.

Table 1. Optimal grating parameters of the METIS VPMs. All designs assume a sidewall angle $\alpha = 2.45$ deg.

Band	period Λ	line width w	depth h
VPM-L (2.9 – 4.1 μm)	1.21 μm	0.65 μm	5.53 μm
VPM-M (3.9 – 5.3 μm)	1.63 μm	0.83 μm	6.55 μm
VPM-N (8.1 – 13.1 μm)	3.40 μm	1.86 μm	17.21 μm

All METIS VPMs are manufactured at the Ångström laboratory of the Uppsala University, using high-purity polycrystalline diamond substrates obtained from Diamond Materials GmbH in Freiburg, Germany. The process begins with laser marking each substrate for identification. Using electron beam lithography, a concentric pattern is etched onto a thin resist film to create the VPM master. This pattern is then transferred onto a silicon (Si) mask using solvent-assisted micromolding (SAMIM). The diamond substrates, coated with the Si mask, undergo deep reactive ion etching (DRIE) in a controlled clean room environment to etch precise grating structures. Following etching, the Si mask is removed, and the VPMs are meticulously cleaned to remove any residues. Forsberg et al.⁸ give a detailed description of the manufacturing of the METIS VPMs.

Quality assurance involves testing the masks on optical benches at the University of Liège (VPM-L and VPM-M) and at CEA Saclay (VPM-N) to verify their performance across specific wavelengths. The final steps potentially include adjusting the VPMs to ensure they meet the specifications, by tuning the grating depth through additional plasma etching if needed. This rigorous process ensures VPMs deliver high performance, and comply with METIS requirements.

3. TESTING VPM-L AND VPM-M

3.1 The VODCA test bench at ULiège

The VODCA (Vortex Optical Demonstrator for Coronagraphic Applications) test bench,⁹ illustrated in Fig. 2, is designed for evaluating the performance of VPMs within a specific spectral range. It operates in the infrared from H to M band ($1.44 - 5.0\mu\text{m}$), utilizing a supercontinuum laser capable of wavelengths up to $4.1\mu\text{m}$ (H to L band). The setup includes both broadband and narrowband filters, along with two quantum cascade lasers covering the M band ($4.5\mu\text{m}$ and $5.0\mu\text{m}$). A deformable mirror is integrated to correct for static aberrations in the system. The optical path of VODCA includes two large parabolic mirrors to direct the beam alternately between pupil and focal planes, effectively minimizing chromatic aberrations. Positioned in an intermediate focal plane, the VPM under evaluation interacts with a beam characterized by an f-number of approximately F/45. Following the third reflection on a parabolic mirror, a Lyot stop restricts diffracted light, reducing the pupil to 75% of its original diameter. The beam, now at F/60, is directed onto a FLIR thermal imaging infrared camera, with a core Airy spot diameter of approximately 12 pixels at $\lambda = 3\mu\text{m}$, and 21 pixels at $\lambda = 5\mu\text{m}$.

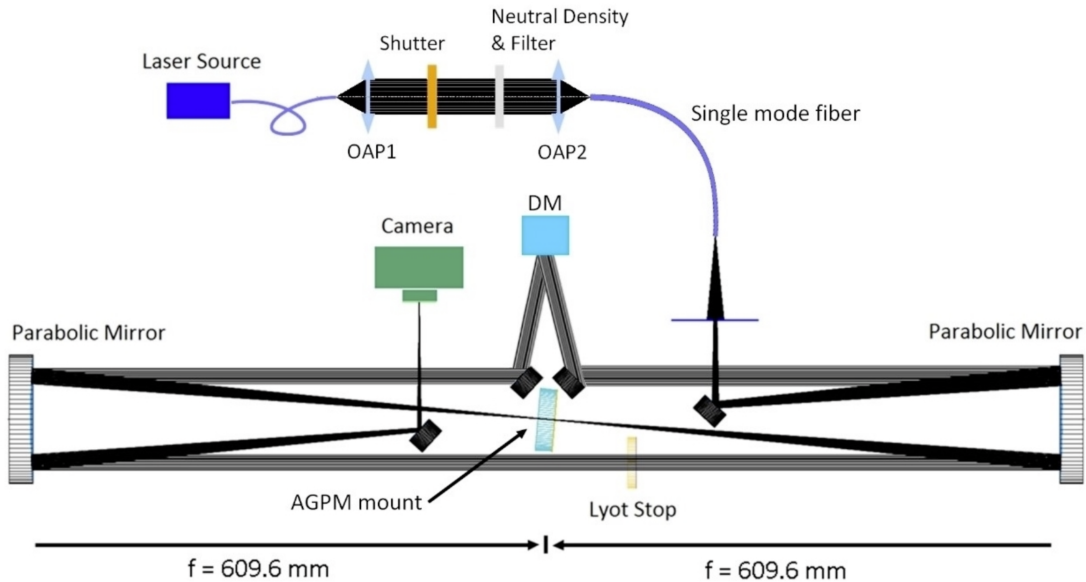


Figure 2. Optical layout of the VODCA coronagraphic test bench at the ULiège STAR Institute (Jolivet et al., 2014).⁹

The test bench methodology involves evaluating VPM performance by measuring their transmission (Sec. 3.2) and their null depth (Sec. 3.3 and Sec. 3.4) as defined by Eq. 3. The null depth measurements are achieved by comparing the flux of a coronagraphic image with that of a reference image obtained by laterally displacing the phase mask in the focal plane. The null depth is calculated as the ratio of fluxes within a specific region of interest, typically defined (in terms of diameter) by the full width at half maximum (FWHM) of the Airy disk. This approach avoids including the effect of low-order aberrations as much as possible.

3.2 Transmission measurements

Fresnel reflections on the internal sides of the VPMs can cause significant power loss. Moreover, those reflections are not properly cancelled out by the vortex effect and can limit the component performance. Multi-layer coatings are expensive and can face adhesion, thermal mismatch, and transparency issues, especially in infrared applications. Instead, two-dimensional antireflective gratings (ARGs) are etched directly onto the backside of the METIS VPMs, minimizing side effects. Those 2D-ARGs are suitable for unpolarized light, are easier to manufacture than traditional coatings and can be designed using RCWA. The backside reflection for diamond around $4\mu\text{m}$ is high at around 17%, but this is significantly reduced to approximately 1% thanks to the ARGs.

To assess the quality of the ARGs and their ability to reduce the ghost signal, the total transmission of the VPMs is measured in various regions far from the vortex center. The transmission is consistently uniform, with a standard deviation of 2-3%. Moreover, the transmission is measured at various wavelength using filters, and compared with the theoretical transmission calculated with RCWA including material absorption, as shown in Fig. 3. The results are highly satisfactory, as the figure demonstrates that the measurements closely align with the theoretical values, indicating that the ghost signal is nearly completely eliminated.

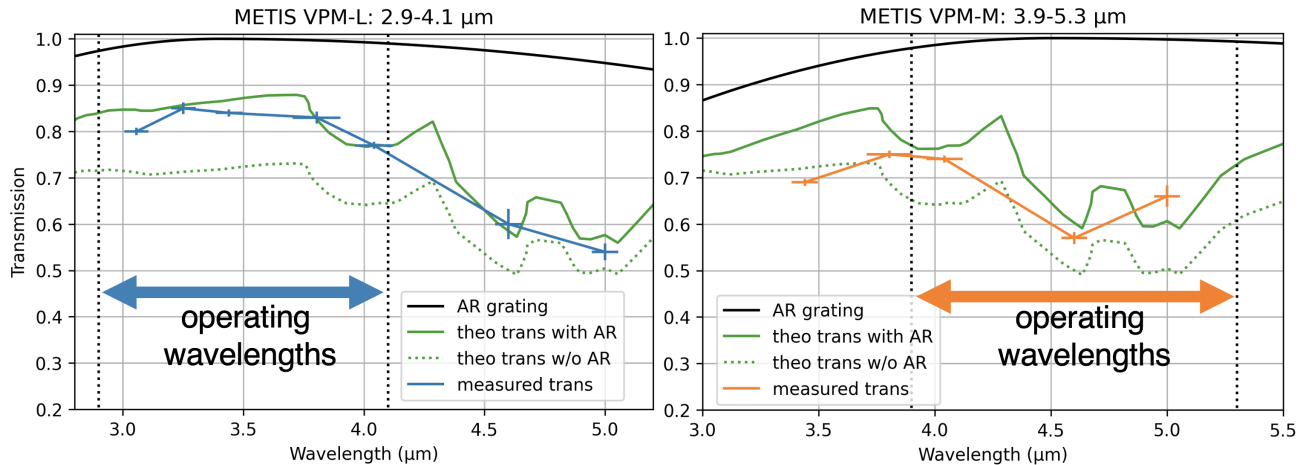


Figure 3. LM-band transmission measurements of VPM-L (left, blue curve) and VPM-M (right, orange curve) with an ARG etched on their backside. The ARG transmission is given by the black curve, optimized for the operating wavelengths of each VPM. The green curves show the calculated theoretical transmissions, with (solid line) and without (dotted line) the ARG. The difference between the black and the green curve corresponds to the intrinsic throughput of a $300\mu\text{m}$ thick slab of CVD diamond.

In a subsequent phase, we investigate the off-axis transmission (OAT) profile as shown in Fig. 4. The OAT is critical for assessing the VPM performance across different angular separations from the star, ensuring that it allows detecting fainter objects close to their host star. The results of these measurements suggest an inner working angle (IWA, defined as the 50% off-axis throughput point of a coronagraphic system) of about $1 \times \lambda/D$, which is in excellent alignment with theoretical expectations,¹⁰ further suggesting that our VPMs effectively produce the expected textbook vortex effect. This result is not representative of the OAT that will be achieved in METIS as it depends on the input pupil shape and Lyot stop design.

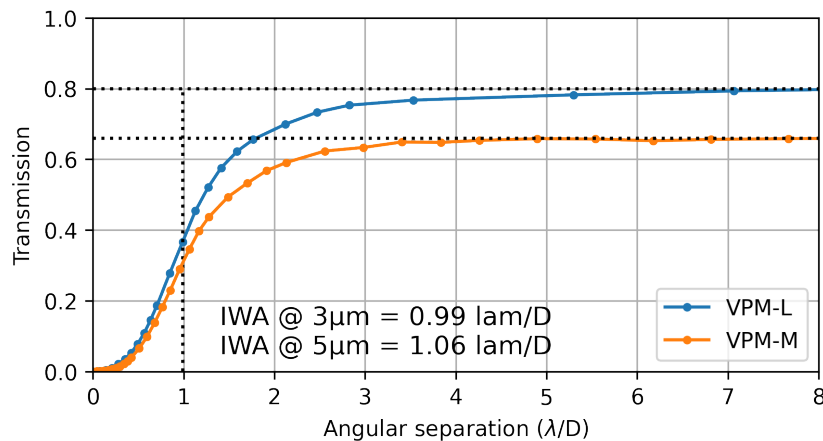


Figure 4. Measured transmission as a function of the angular separation between the beam and VPM centre, expressed in resolution elements (λ/D).

3.3 VPM-L null depth measurements

VPM-L demonstrates excellent performance as shown in Fig. 5, meeting the stringent METIS requirements, here expressed in terms of rejection R (i.e., the inverse of null depth):

- VPM-L achieves a mean R greater than 800 (requirement = 500);
- the minimum R exceeds 500 everywhere at L band (requirement = 100).

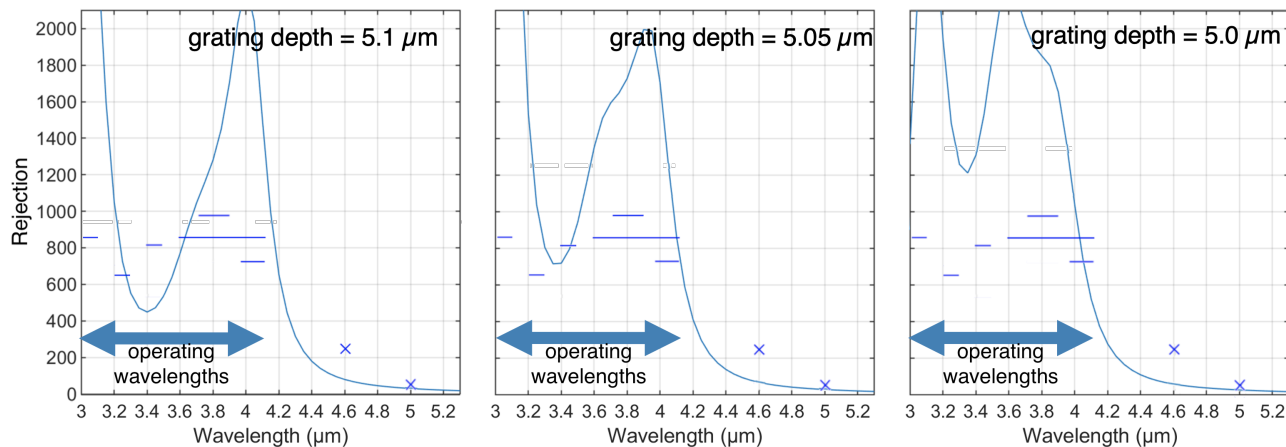


Figure 5. Rejection (i.e., the inverse of null depth) of VPM-L. The horizontal lines at L band and the crosses at M band indicate the measurements on VODCA, and are identical on the 3 graphs. Only the continuous RCWA rejection profiles differ: the middle graph corresponds to our best estimation of the grating parameters (depth of $5.05\mu\text{m}$), while the other two graphs show the expected rejection with slightly varying grating depths.

Grating parameters such as line width and grating depth are meticulously estimated by combining scanning electron microscopy (SEM) and null depth measurements. The line width is approximately $0.655\mu\text{m}$, while the grating depth is estimated to be around $5.05\mu\text{m}$. Based on those estimated parameters, continuous rejection profiles are calculated using RCWA for slightly different grating design scenarios, further ensuring compliance of VPM-L performance.

3.4 VPM-M null depth measurements

Concerning the VPM-M component, the initial measurements were significantly below expectations, with the rejection rate barely reaching 20 in the M band (see Fig. 6, left). This low performance was expected, as the etch depth was known to be too large in the initial manufacturing. Through careful analysis, we have confirmed that the gratings were approximately 800nm too deep. To address this issue, the component was returned to the manufacturer in Uppsala for a re-etching process,¹¹ which aimed to reduce the depth of the grooves by about 800nm . Once the re-etching process was completed, the component was sent back to ULiège for retesting.

The retesting on the VODCA test bench is crucial to ensure that the adjustments have successfully corrected the grating parameters. After the re-etching and subsequent testing, we now confirm that the performance of VPM-M is significantly improved (see Fig. 6, right). The measured results indicate that VPM-M appears to meet the stringent requirements of the METIS instrument over the $4.3 - 5.3\mu\text{m}$ range, with a rejection rate exceeding 300 at a wavelength of $4.6\mu\text{m}$ and over 900 at $5\mu\text{m}$. These improved measurements confirm that the re-etching process can effectively address manufacturing issues, resulting in a component that performs as required.

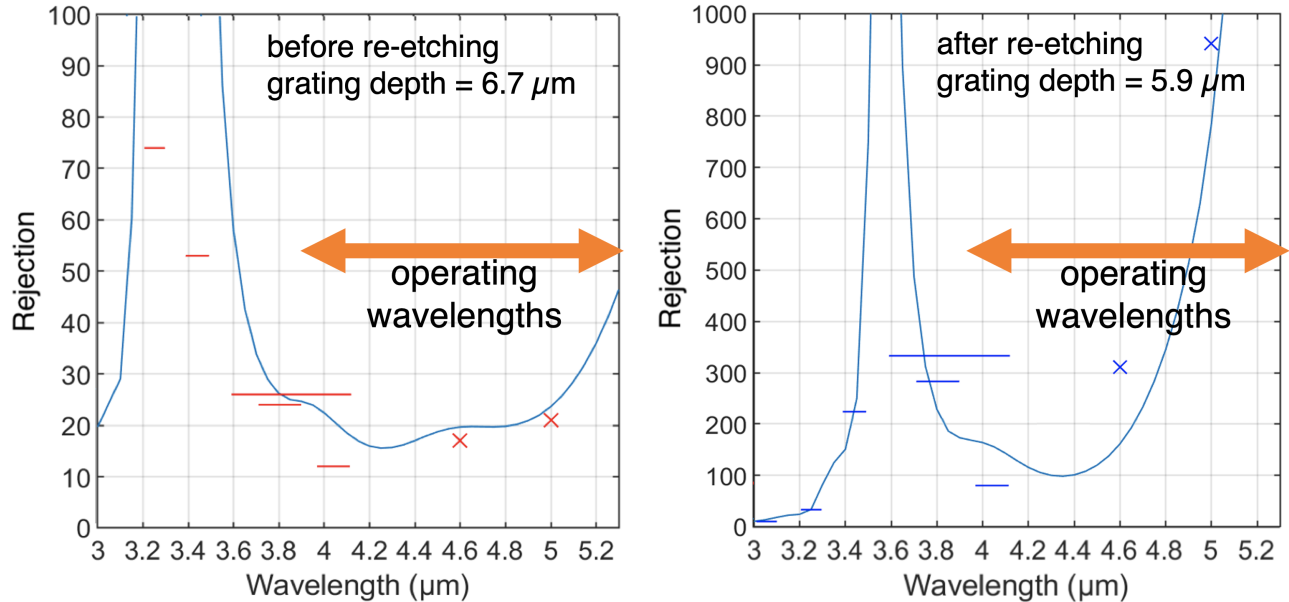


Figure 6. Rejection (i.e., the inverse of null depth) of METIS VPM-M. The horizontal lines at L band and the crosses at M band indicate the measurements on VODCA. Left graph: initial poor performance before re-etching. Right graph: improved performance after re-etching 800nm shallower.

4. TESTING VPM-N

4.1 The cryogenic test bench at CEA Saclay

A test bench¹² at the Department of Astrophysics at CEA (Saclay, France), previously used for testing the JWST/MIRI imager, has been significantly refurbished to meet the requirements for VPM-N tests. This setup includes IR laser sources, a motorized hexapod with micrometric accuracy, and a telescope simulator with adjustable pupil shape and position. The bench uses a cryogenic facility to hold an infrared imager (the MIRI imager Engineering and Test Model) with an Aquarius detector. Uppsala University fabricated three VPMs, which were delivered to CEA in 2023.

4.2 VPM-N null depth measurements

In this section, we report on the results of tests conducted on the three VPM-N manufactured for METIS, with a focus on measuring rejection levels. All VPM-N must achieve an average rejection level across the entire band greater than 100 and a rejection greater than 20 at any wavelength to be considered acceptable.

Data acquisition involves capturing off-axis and on-axis images at various wavelengths for all VPMs, using the NGC system for real-time PSF observation and automated micro-scans around the mask center for precise measurements. Analysis methods include comparing the encircled energy of reference and coronagraphic PSFs, with additional considerations for photometric stability and spatial non-homogeneity.

Similarly to VPM-M described in Sec. 3.4, initial measurements indicated that two VPM-N did not meet the required rejection levels due to incorrect grating depths. After re-etching at Uppsala University to reduce the grating depths by approximately 800nm, retesting showed significant improvement, as illustrated on Fig. 7, with rejection rates above 100 at all wavelengths meeting the METIS requirements comfortably. The peak rejections appear around 11 – 12μm as predicted by the RCWA simulations (Fig. 1).

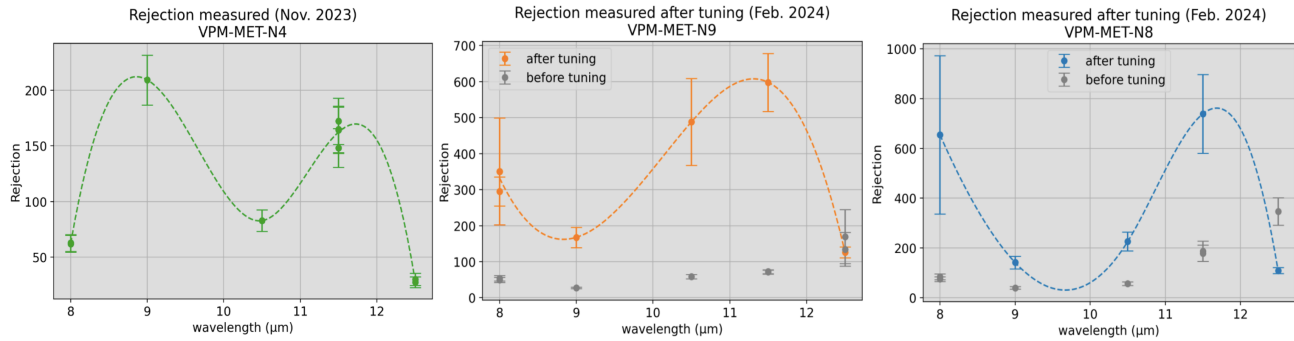


Figure 7. Rejection (i.e., the inverse of null depth) of three METIS VPM-N components. Only one (left graph) was compliant after first run, the other 2 needed re-etching/tuning. The dotted lines are merely spline interpolations intended to guide the viewer’s eye and do not represent a model for the rejection.

5. CONCLUSIONS

In this paper, we have described the design and manufacturing of METIS VPMs, and presented their performance evaluated on two optical testbeds, confirming the compliance to the METIS requirements. In particular, the VPM-L demonstrates notable performance, exceeding the requirements with a mean rejection greater than 800, indicating successful alignment of manufacturing with design specifications.

A critical aspect of this project was the successful re-etching of VPM-M and VPM-N components. Initially, discrepancies in grating depths led to subpar performance. However, the iterative re-etching process, which involved precise removal of approximately 800nm from the grating depths, proved to be highly effective. Post re-etching, both VPM-M and VPM-N components exhibited substantial performance improvements, meeting and even exceeding the contrast requirements set by METIS. This emphasizes the importance of precise manufacturing adjustments and highlights the robustness of the iterative testing and manufacturing approach adopted in this project.

ACKNOWLEDGMENTS

This project has received funding from the European Research Council (ERC) under the European Union’s Horizon 2020 research and innovation programme (grant agreement No 819155), and from the Wallonia-Brussels Federation (grant for Concerted Research Actions).

REFERENCES

- [1] Mawet, D., Riaud, P., Absil, O., and Surdej, J., “Annular groove phase mask coronagraph,” *The Astrophysical Journal* **633**, 1191 (nov 2005).
- [2] Carlomagno, B., Delacroix, C., Absil, O., Cantalloube, F., de Xivry, G. O., Pathak, P., Agocs, T., Bertram, T., Brandl, B., Burtscher, L., Doelman, D., Feldt, M., Glauser, A., Hippler, S., Kenworthy, M., Por, E., Snik, F., Stuik, R., and van Boekel, R., “METIS high-contrast imaging: design and expected performance (Erratum),” *Journal of Astronomical Telescopes, Instruments, and Systems* **6**, 049801 (Oct. 2020).
- [3] Delacroix, C., Absil, O., de Xivry, G. O., Shinde, M., Pathak, P., Cantalloube, F., Carlomagno, B., Christiaens, V., Boné, A., Dolken, D., Kenworthy, M., and Doelman, D., “The High-contrast End-to-End Performance Simulator (HEEPS): influence of ELT/METIS instrumental effects,” in [*Modeling, Systems Engineering, and Project Management for Astronomy X*], Angeli, G. Z. and Dierickx, P., eds., **12187**, 121870F, International Society for Optics and Photonics, SPIE (2022).
- [4] Brandl, B., Absil, O., Feldt, M., Garcia, P., Glasse, A., Guedel, M., Labadie, L., Meyer, M., Pantin, E., Quanz, S., Wang, S.-Y., van Winckel, H., Bettonvil, F., Glauser, A. M., van Boekel, R., Salo, C., Scheithauer, S., Stuik, R., Haupt, C., and Siebenmorgen, R., “Final design and status of the Mid-Infrared ELT Imager and Spectrograph, METIS,” *Proc. SPIE*, 13096–38 (2024).

- [5] Absil, O., Kenworthy, M., Delacroix, C., Orban de Xivry, G., König, L., Pathak, P., Doelman, D., Por, E., Snik, F., Cantalloube, F., Carlotti, A., Courtney-Barrer, B., Dolkens, D., Glauser, A., van Boekel, R., Bertram, T., Feldt, M., Pantin, E., Quanz, S., Bettonvil, F., and Brandl, B., “Metis high-contrast imaging: from final design to manufacturing and testing,” in [*Advances in Optical and Mechanical Technologies for Telescopes and Instrumentation VI*], *Proceedings of the SPIE* **13096**, SPIE (2024).
- [6] Absil, O., Delacroix, C., Orban de Xivry, G., Pathak, P., Willson, M., Berio, P., van Boekel, R., Matter, A., Defrère, D., Burtscher, L., Woillez, J., and Brandl, B., “Impact of water vapor seeing on mid-infrared high-contrast imaging at ELT scale,” in [*Adaptive Optics Systems VIII*], Schreiber, L., Schmidt, D., and Vernet, E., eds., *Society of Photo-Optical Instrumentation Engineers (SPIE) Conference Series* **12185**, 1218511 (Aug. 2022).
- [7] Delacroix, C., Forsberg, P., Karlsson, M., Mawet, D., Absil, O., Hanot, C., Surdej, J., and Habraken, S., “Design, manufacturing, and performance analysis of mid-infrared achromatic half-wave plates with diamond subwavelength gratings,” *Appl. Opt.* **51**, 5897–5902 (Aug 2012).
- [8] Forsberg, P., Karvinen, P., Ronayette, S., Kuittinen, M., Absil, O., König, L., Delacroix, C., Orban de Xivry, G., Barrière, J.-C., Pantin, E., and Karlsson, M., “Making the diamond vortex phase masks for the metis instrument,” *Diamond and Related Materials* **146**, 111237 (2024).
- [9] Jolivet, A., Piron, P., Huby, E., Absil, O., Delacroix, C., Mawet, D., Surdej, J., and Habraken, S., “The VORTEX coronagraphic test bench,” in [*Advances in Optical and Mechanical Technologies for Telescopes and Instrumentation*], Navarro, R., Cunningham, C. R., and Barto, A. A., eds., **9151**, 91515P, International Society for Optics and Photonics, SPIE (2014).
- [10] Riaud, P. and Hanot, C., “Combining coronagraphy with interferometry as a tool for measuring stellar diameters,” *The Astrophysical Journal* **719**, 749 (jul 2010).
- [11] Vargas Catalán, E., Huby, E., Forsberg, P., Jolivet, A., Baudoz, P., Carlomagno, B., Delacroix, C., Habraken, S., Mawet, D., Surdej, J., Absil, O., and Karlsson, M., “Optimizing the subwavelength grating of l-band annular groove phase masks for high coronagraphic performance,” *A&A* **595**, A127 (2016).
- [12] Ronayette, S., Mouzali, S., Barrière, J.-C., Pantin, É., Orduna, T., Gallais, P., Lortholary, M., Dumaye, L., Absil, O., Delacroix, C., Ives, D., and Karlsson, M., “An N-band test bench for the METIS coronagraphic masks,” in [*Ground-based and Airborne Instrumentation for Astronomy VIII*], Evans, C. J., Bryant, J. J., and Motohara, K., eds., **11447**, 114472U, International Society for Optics and Photonics, SPIE (2020).